



Ballistic crossfield ion beam propagation in a magnetoplasma

K. Papadopoulos, A. Mankofsky, R. C. Davidson, and A. T. Drobot

Citation: *Physics of Fluids B: Plasma Physics (1989-1993)* **3**, 1075 (1991); doi: 10.1063/1.859836

View online: <http://dx.doi.org/10.1063/1.859836>

View Table of Contents: <http://scitation.aip.org/content/aip/journal/pofb/3/4?ver=pdfcov>

Published by the [AIP Publishing](#)

Articles you may be interested in

[Formation and stability of polarization sheaths of a crossfield beam](#)

Phys. Fluids B **4**, 1033 (1992); 10.1063/1.860226

[Limits on the crossfield propagation of streams of cold plasma](#)

Phys. Fluids **30**, 2518 (1987); 10.1063/1.866090

[Crossfield free electron laser instability for a tenuous electron beam](#)

Phys. Fluids **27**, 233 (1984); 10.1063/1.864518

[Crossfield currentdriven modified ioncyclotron instability in an inhomogeneous magnetoplasma](#)

Appl. Phys. Lett. **25**, 637 (1974); 10.1063/1.1655339

[CrossField Diffusion of Quiescent Potassium Magnetoplasmas](#)

Phys. Fluids **9**, 2294 (1966); 10.1063/1.1761609

Ballistic cross-field ion beam propagation in a magnetoplasma

K. Papadopoulos,^{a)} A. Mankofsky, R. C. Davidson,^{b)} and A. T. Drobot
Science Applications International Corporation, 1710 Goodridge Drive, McLean, Virginia 22102

(Received 15 March 1990; accepted 15 November 1990)

Long range cross-field ion beam propagation in a magnetoplasma has been studied in the high kinetic beta regime by using computer simulations and analytic techniques. A new regime of long range ballistic beam propagation has been discovered for narrow high-density beams. Ion beams with transverse size $\Delta \ll R_b$, where R_b is the ion beam gyroradius and mass density $n_b M_b \gg n_p M_p$, where $n_b (M_b), n_p (M_p)$ are the particle density (mass) of the beam and the ambient ions can propagate ballistically across the ambient magnetic field over distances varying from a minimum of $(n_b/n_p)R_b$ to over an order of magnitude longer depending on the extent of initial interpenetration of the beam and the background plasma. The propagation mode is characterized by the formation of a front at the head of the beam, which forces the plasma to move sideways and prevents beam-plasma interpenetration. The system momentum is locally balanced by a corresponding displacement of the head of the beam in the opposite direction to the plasma, which is equivalent to erosion of the beam front. The physics of the interaction is distinct from the conventional magnetohydrodynamic picture and requires kinetic treatment for beam ions. Scaling laws that can be tested by laboratory and space experiments are presented.

I. INTRODUCTION

The propagation of high-speed neutralized ion beams, often called plasmoids, across a magnetic field is among the oldest of problems in plasma physics. It first arose in investigations of the origin of magnetospheric storms and substorms.^{1,2} Despite the long history of investigation, a clear model has yet to emerge. Early theoretical models established by Chapman and Ferraro,¹ Ferraro,² Tuck,³ and Chapman,⁴ indicated that a neutralized beam with a large width Δ transverse to the ambient magnetic field \mathbf{B}_0 ($\Delta \gg R_b$, where R_b is the gyroradius of the beam ions), will, in general, compress the magnetic field but will not propagate significantly. Propagation can potentially occur in the diamagnetic regime when $\beta_b \equiv 4\pi n_b M_b u_b^2 / B_0^2 \gg 1$, where n_b, M_b , and u_b are the density, mass, and cross-field velocity of the beam ions. This propagation mode can be properly described by magnetohydrodynamics (MHD) and is equivalent to the propagation of a solid conductor moving across \mathbf{B}_0 . During propagation, the beam picks up and carries along the ambient plasma and magnetic field, in a fashion similar to the pickup of cometary ions by the solar wind.⁵ The mass loading, along with the various pickup ring instabilities, soon destroys the beam coherence. Such models emphasize the diamagnetic properties of the plasma.

Nondiamagnetic models were established by Bostick,⁶ Schmidt,⁷ Dolique,⁸ Baker and Hammel,⁹ Baribaud *et al.*,¹⁰ and Livesey and Pritchett.¹¹ These models addressed issues related with low ($\beta_b \ll 1$) to moderate ($\beta_b \sim 1-3$) values of β_b . Of critical importance were the theoretical investigation of Schmidt,⁷ and the experimental results of Baker and Hammel.⁹ They addressed the propagation of neutralized

ion beams across a magnetic field for low β_b ($\beta_b < 1$), and for narrow beams in the sense $R_e, c/\omega_e < \Delta \ll R_b$, where R_e is the electron gyroradius and ω_e is the plasma frequency. In this case the flow energy is not sufficient to alter the magnetic field configuration; therefore the ambient magnetic field controls the electron and ion dynamics. A polarization electric field develops by the differential motion of the magnetized electrons ($R_e \ll \Delta$) and the unmagnetized ions ($R_b > \Delta$). The polarization field \mathbf{E} , coupled with the ambient field \mathbf{B}_0 , allows the neutralized beam to move by an $\mathbf{E} \times \mathbf{B}_0$ drift.⁷ This mode of propagation was experimentally observed by Baker and Hammel.⁹ Peter and Rostoker¹² noted that dielectric shielding as a result of the presence of an ambient plasma does not affect the beam propagation as long as $\Delta > R_b/\epsilon_p$, where ϵ_p is the low-frequency dielectric constant of the plasma in the region occupied by the beam. This is equivalent to the condition $V_{Ap}/V_{Ab} < 1$, where V_{Ab}, V_{Ap} are the beam and plasma Alfvén speeds. Scholer's¹³ model of artificial propagation of ion clouds in the magnetosphere belongs to this class of low kinetic β_b , sub-Alfvénic propagation modes.

The propagation of neutralized ion beams was studied in a series of recent experiments in the range of $0.01 < \beta_b < 300$ and for various plasma pressures.¹⁴ It was found that the magnetic field penetrated very quickly into the beam and for a range of ambient plasma pressures undeflected propagation of the ion beam was accomplished. The propagation deteriorated at high plasma pressures corresponding to $n_b/n_p < 1$, where n_b, n_p are the beam and plasma density correspondingly. Unfortunately the experimental length was of the order of or less than the ion gyroradius, making it difficult to interpret the results.

Anomalous processes are also thought to play an important role in ion beam propagation. Evidence comes from an experiment by Birko and Kirchenko¹⁵ in which an ion

^{a)} Permanent address: Department of Physics and Astronomy, University of Maryland, College Park, Maryland 20742.

^{b)} Permanent address: Plasma Physics Laboratory, Princeton University, Princeton, New Jersey 08543.

acoustic wave was driven unstable on the surface of a low-energy beam in the $\beta_b < 1$ regime, apparently resulting from the relative drift between heavy and light ions. A similar phenomenon was observed in two-dimensional (2-D) particle simulations of cross-field ion beam propagation.¹⁶ In this case, the wave excitation was attributed to the Buneman instability. The surface wave penetrated throughout the bulk of the plasma and was accompanied by strong electron heating and dispersal of the beam. The above result was for the case where the magnetic field was perpendicular to the simulation plane. In another case where the field was in the simulation plane, many new effects were observed. Among them, formation of a strong diamagnetic cavity was accompanied by strong beam focusing. Some, rather unreliable as a result of low resolution, 3-D simulation results indicate a weaker focusing effect.

Experimental data on cross-field ion beam propagation under ionospheric and magnetospheric conditions are mainly due to two recent neutral gas injection experiments, AMPTE,¹⁷⁻²⁰ and Porcupine²¹ and from photographs taken following the Starfish nuclear explosion in 1962. The most important result of the AMPTE injection is the formation of a diamagnetic cavity for the release upstream of the bow shock in the solar wind under conditions equivalent to $\beta_b \gg 1$. In the release frame, the solar wind slowed down from 550 km/sec to almost zero, at which point it was diverted sideways around the release. The dominant interaction between the solar wind and the finite radius barium cloud occurred ahead of the cavity, and was consistent with the excitation of ion and electron cross-field streaming instabilities. The diagnostics could not determine whether interpenetration of the solar wind and the main cloud occurred at early times. There was substantial electron and proton heating in the interaction. For details and analysis, see Papadopoulos and Lui.²⁰ The most important aspect of the Porcupine experiment was the fast penetration of the magnetic field inside the injected xenon ion beam, which was attributed to an anomalous resistivity of the order of the lower hybrid frequency.²¹ Finally, the most impressive aspect of the Starfish photographs is the existence of the so-called jets. These have been interpreted as ion jets composed of bomb debris that propagated over distances greater than 2000 km across the geomagnetic field. A similar effect has been observed in a recent laser experiment at the Naval Research Laboratory.²²

The rather confusing state of the experimental and theoretical results discussed previously is mainly due to a wide range of conditions under which the various experiments were performed and the constraints restricting the validity of the various theories. In addition to the critical role of the value of β_b mentioned previously, many other dimensionless ratios, such as R_b/Δ , $c/\omega_e \Delta$, n_b/n_p , and V_{Ab}/V_{Ap} play an important role in determining the controlling physical processes. Furthermore, most of the experimental measurements are descriptive of transient conditions, while many of the theories address the steady state or even the asymptotic regime. It is the purpose of this paper to examine the propagation of dense ($n_b > n_p$), high β_b ($\beta_b \gg 1$), narrow ($R_e, c/\omega_e \ll \Delta < u_b/\Omega_0 \equiv R_0$) neutralized ion beams by two-

dimensional computer simulations using a hybrid code.²³ The simulation results are utilized to produce an understanding of the underlying physical processes and their sensitivity to changes in the parameters. Emphasis is placed in deriving scaling laws. Although the simulations were performed for parameters relevant to the propagation of neutralized proton beams in the F region of the ionosphere, as will be shown in a later section, the results have much wider applicability.

II. STATEMENT OF PROBLEM: SIMPLIFICATION, PHYSICAL DESCRIPTION, AND ISSUES

Consider a cold, dense ($n_b \gg n_p$), high kinetic beta ($\beta_b \gg 1$) neutralized ion beam injected into a magneto-plasma perpendicular to the direction of the ambient magnetic field $\mathbf{B} = \hat{z} B_0$. The beam has finite dimensions in the x and y directions given by Δ and L_{\perp} , while its length in the z direction is determined by the injection time τ [Fig. 1(a)]. The purpose of the study is to determine the range of ballistic beam propagation, i.e., the range over which the beam propagates undeflected by the presence of the ambient magnetic field and plasma. It is obvious that the problem is a three-dimensional one and includes a multitude of time and length scales. Our approach is to divide the problem into a set of simpler problems whose physical understanding can lead to the desired answers. This approach allows for the identification of key uncertainties that can be addressed by properly designed laboratory or space experiments.

On the shortest time scale of the problem the dominant issue is the charge neutralization of the ion beam when injected in the plasma. This issue is not dealt with here. We

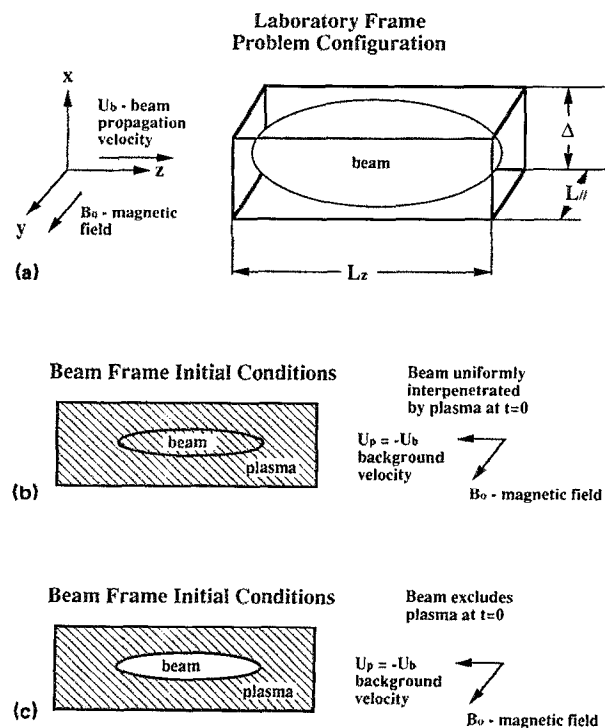


FIG. 1. (a) Problem configuration and (b) and (c) initial conditions.

simply assume that the ion beam is charge and current neutralized on the fastest time scale of the problem. For neutral gas releases in space such as AMPTE or the upcoming NASA program CRRES, neutralization is automatic since the beam is created through the ionization of a neutral gas cloud. For beam injection from ion accelerators the situation is more complex and has been examined by Humphries²⁴ and Brandon.²⁵ As a rule for injection of energetic ion beams in very dilute plasmas charge and current neutralization is achieved very quickly by ejection of electrons from the ion gun region. For injection into dense plasmas neutralization is achieved by flow of ambient electrons.

Another early time issue that could affect the interpretation of the results is the initial conditions under which the simulations were performed. The system can have the following extreme states at $t = 0$ [Figs. 1(b) and 1(c)]: (i) the magnetoplasma is homogeneously distributed inside and outside the beam; (ii) the magnetoplasma has been completely excluded from the beam region. It is, of course, possible to have any intermediate level of penetration between the above extremes. It will be shown that the asymptotic beam propagation for the range of parameters mentioned in the Introduction is independent of the initial configuration. An obvious case consistent with state (i) is again an ion beam created by sudden ionization of a stationary or neutral cloud. Case (ii) can occur on at least short time scales during ion beam injection experiments for at least some injection and plasma parameters.

For the case of beam propagation across an ambient magnetic field the problem is essentially a two-dimensional one since the dynamics of the beam particles in the direction parallel to the magnetic field can be decoupled from the dynamics in the perpendicular direction, at least in the small electron gyroradius limit. In fact this is not strictly correct. If the beam is expanding parallel to the magnetic field direction the beam density decreases with time. Since, as we will see, the cross-field propagation range depends on the ratio n_b/n_p and on β_b , which will vary as a result of field aligned expansion, the two-dimensional model is valid only as long as the expansion is slow enough to maintain $n_b/n_p \gg 1$ and $\beta_b \gg 1$ over the propagation time. We will return to this point later. Another constraint of the two-dimensionality of the simulations is caused by the magnetic field polarization with respect to the simulation plane. If the magnetic field points perpendicular to the simulation plane, i.e., in the direction of the ignored coordinate, then plasma motion around the beam is possible, allowing for the development of self-consistent flow without interpenetration of the beam with the ambient magnetoplasma. This is not the case if the magnetic field is in the simulation plane [i.e., if $\mathbf{B} = \hat{e}_x B_x$ in Fig. 1(a)]. In this case, although flow might develop in the y direction, it cannot flow around the beam since this simulation configuration has implicitly assumed that the beam is infinitely wide in the y direction. Such a configuration will produce unrealistic results for a finite beam in the y direction and care should be exercised in their interpretation.

A final issue concerns the role of turbulent processes driven by local microinstabilities. Such instabilities arise in regions of interpenetration of the beam with the ambient

magnetoplasma or for the case of injection of a beam into vacuum in regions where diamagnetic currents are induced. It should be noted that as a result of the existence of overall inhomogeneities and the associated nonlocal wave transport the microinstability-induced turbulence is not a key factor, except under particular circumstances. The hybrid code utilized allows for sensitivity studies of the role of anomalous transport since the value of the electron-ion collision frequency can be varied. Such studies were first performed in the hybrid simulations of the Earth's bow shock with very satisfactory results.^{26,27} Furthermore, the hybrid code gives the value of local cross-field currents and thus allows for an assessment of the possible excitation of microturbulence.

With the previous remarks in mind we proceed to discuss the simulation results for the case of cross-field injection of a neutralized finite size beam, which at $t = 0$ was completely penetrated by the ambient magnetoplasma. The results will serve to establish the physics ground rules under which the role of the remaining issues can be assessed, and a comprehensive model of the ion cross field propagation can emerge.

III. HYBRID SIMULATION RESULTS FOR $\mathbf{B} = \hat{e}_y B_0$

A set of two-dimensional computer simulations was performed using CIDER, a two-dimensional hybrid code whose detailed description can be found in Mankofsky *et al.*²³ Briefly, the ions are treated as discrete particles using standard particle-in-cell techniques to follow their motion in the electromagnetic (em) fields. Summing over the particles provides the ion charge and current density. The electrons are treated as a massless fluid, described via the momentum and energy equations. These equations, along with the ion equations of motion, are solved self-consistently on a uniform two-dimensional grid for the ion velocity vectors, the em fields, and the electron pressure, in the nonradiative limit (i.e., Darwin Hamiltonian).

The equations solved in the simulation are

$$\frac{1}{c} \frac{\partial}{\partial t} \mathbf{B} = -\nabla \times \mathbf{E} \quad (1)$$

and

$$\nabla \times \mathbf{B} = (4\pi/c)(\mathbf{J}_e + \mathbf{J}_i), \quad (2)$$

where \mathbf{J}_e and \mathbf{J}_i are the corresponding electron and ion current densities. The first equation, Faraday's Law, is used to determine the change in magnetic field caused by inductive electric fields. In the second equation, Ampère's law, the displacement current has been neglected, implying that $\nabla \cdot (\mathbf{J}_e + \mathbf{J}_i) = 0$. This in conjunction with quasineutrality, $n_e \cong n_i$, permits the determination of the velocity \mathbf{u}_e of the electron fluid as a function of the magnetic field and ion current density. Furthermore, neglecting electron inertia, but retaining electron pressure and collisionality, the electric field is found from force balance for the electrons using the generalized Ohm's law,

$$\mathbf{E} = -\frac{\mathbf{u}_e}{c} \times \mathbf{B} - \frac{\nabla P_e}{n_i |e|} - \frac{m_e}{|e|} \sum_s \nu_{es} (\mathbf{u}_e - \mathbf{u}_{es}). \quad (3)$$

Here P_e is the electron pressure determined from an appro-

appropriate electron energy equation and ν_{es} is the effective collision frequency with specie "s." The collision frequency can be based on a classical Coulomb interaction or used to account for nonlinear plasma coupling through the use of an anomalous prescription. The electric field contains both an electrostatic as well as an inductive component. This model can account for an extremely large range of physical phenomena. It includes ambipolar expansion, magnetic field convection, and magnetic field diffusion. The model resolves Alfvén waves, whistlers, and kinetic ion effects, but because it is explicit it leads to the limitation $\Delta t v^* < \Delta x$, where Δt is the time step, Δx is the smallest cell size, while v^* is the maximum of the Alfvén and whistler wave phase velocities or the fastest ion velocity in the problem. The neglect of electron inertia does not allow a proper treatment of the electron skin depth so our results are valid only for scale lengths much greater than c/ω_e .

The system used in the ion beam simulations has periodic boundary conditions in the direction transverse to the flow (i.e., the x axis). In the flow direction (z axis) plasma is injected from the right boundary at a rate $n_0 u_b$ and permitted to leave on the left at the local flux rate. The magnetic field is allowed to float at these boundaries. We describe below simulation results designed to illustrate quantitatively aspects of the high β_b propagation model.

In the simulations presented here, the ambient plasma was composed of O^+ with density $n_p = 10^5 \text{ \#/cm}^3$ and temperature 0.25 eV, and was embedded in a magnetic field $B_0 = 0.3 \text{ G}$. These are parameters typical of the ionospheric F region. The beam was composed of protons and was given a Gaussian profile in the x and z directions. Beam velocities $u_b = 10^8, 2 \times 10^8, \text{ and } 4 \times 10^8 \text{ cm/sec}$ were studied, while the total number of beam particles varied between $10^{17} - 10^{19}$, corresponding to peak beam densities in the range of $n_b \approx 5 \times 10^6 - 8 \times 10^7 \text{ \#/cm}^3$. Table I lists the parameters of the simulation runs in real (dimensional) and dimensionless units. The runs described here were performed with the magnetic field B_0 out of the plane of the simulation. All the simulations were performed in the beam reference frame. In this frame, the beam particles are initially stationary while the magnetoplasma flows with $\mathbf{u} = -u_b \hat{e}_z$, with the aid of an appropriate motional electric field. The geometry and the initial conditions of the beam in the simulations are shown in Figs. 2(a)–2(c). Figure 2(a) shows the beam isodensity contours at $t = 0$. To facilitate the understanding of the physics, diagnostic cuts at the positions labeled 1–5 were taken along the x and z axes. Figures 2(b) and 2(c) show the

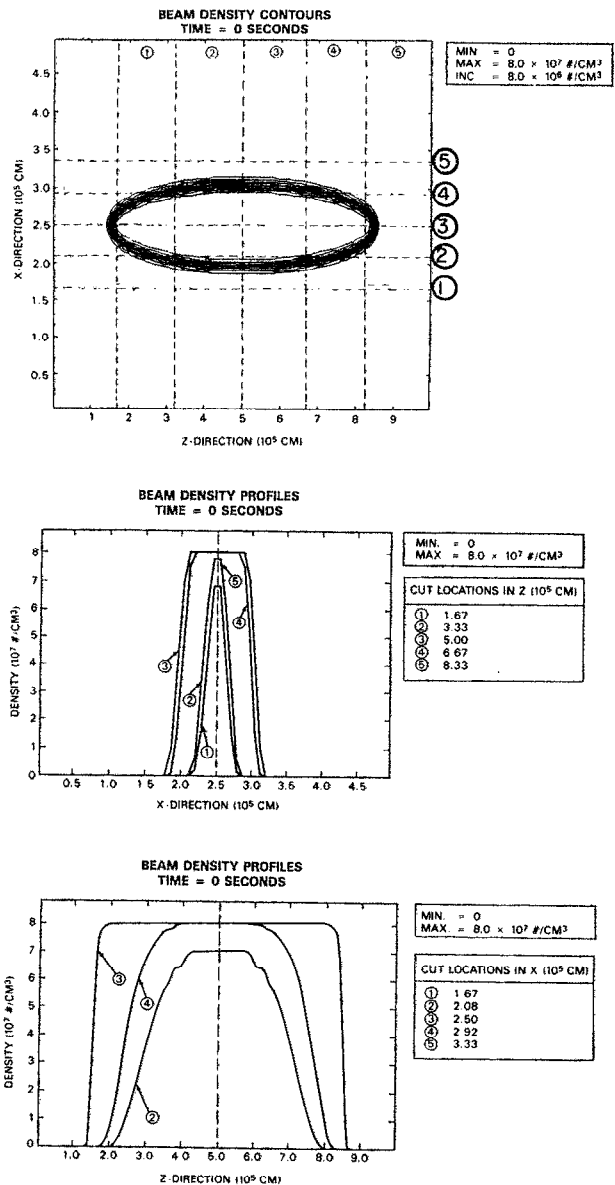


FIG. 2. Initial beam profiles for all runs. The parameters correspond to run #1. For the other runs they can be scaled according to the value of the peak beam density n_b . (a) Beam isodensity contours. This figure also shows the locations of the vertical and horizontal diagnostic cuts in the (x - z) plane. (b) Beam density profiles along vertical cuts 1–5. (c) Beam density profiles along horizontal cuts 1–5.

TABLE I. Parameters used for beam propagation simulations.

| Run # | Beam velocity (10^8 cm/sec) | Total # of beam particles (10^{17}) | Peak beam density n_b (10^6 \#/cm^3) | n_b/n_0 | V_b/V_A |
|-------|--|--|--|-----------|-----------|
| 1 | 1 | 48 | 80 | 800 | 1.7 |
| 2 | 2 | 48 | 80 | 800 | 3.4 |
| 3 | 4 | 48 | 80 | 800 | 6.8 |
| 4 | 1 | 12 | 20 | 200 | 1.7 |
| 5 | 1 | 3 | 5 | 50 | 1.7 |

initial beam profiles for cuts 1–5 along the x and z axes. The basic physics of the interaction becomes clear by referring in detail to one of the runs of Table I. Run #1 is examined first. Computer time constraints resulting from the explicit nature of the codes limited the runs to time $t \leq 2.5 \text{ msec}$, which corresponds to $\Omega_b t \approx 8$ or propagation distances of $8R_b$ ($\Omega_b = eB_0/M_b c = 3 \times 10^3 \text{ sec}^{-1}$ is the proton cyclotron frequency).

The evolution of the beam for the parameters of run #1 can be seen from Figs. 3(a) and 3(b) and Figs. 4(a) and 4(b). Figures 3(a) and 3(b) show the beam isodensity contours at times $t = 1.25$ and 2.5 msec , corresponding to

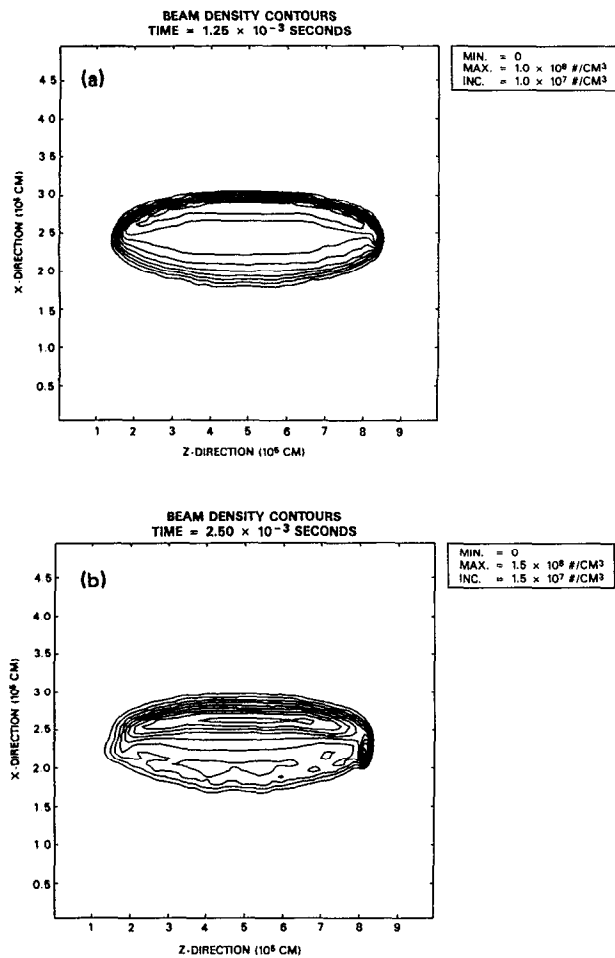


FIG. 3. Isodensity beam contours for run #1. (a) At $t = 1.25$ msec (equivalently $\Omega_b t = 4$ or propagation distance $4R_b$). (b) At $t = 2.5$ msec.

$\Omega_b t = 4$ and 8 and equivalent beam propagation distances of $4R_b$ and $8R_b$. It is clear that the beam has been deformed but has maintained its macroscopic integrity as a plasmoid and followed a ballistic trajectory. Similar conclusions are derived from Figs. 4(a) and 4(b), which show the beam profiles as a function of x at the diagnostic cuts. Figures 4(a) and 4(b) should be compared with Fig. 2(b) at $t = 0$. Notice that both the isodensity contours and the density profiles show density compression at the center of the beam by almost a factor of 2 (the vertical scale in the figures changes according to the peak value). Detailed examination of Fig. 4(b) shows the presence of a secondary density peak at the front of the beam (position #5), which is displaced downward (i.e., in the negative x direction). This corresponds to erosion of the beam front and is also apparent at the front in Fig. 3(b). Figures 5(a) and 5(b) show the profile of the plasma flow velocity at the horizontal diagnostic cuts for times $t = 1.25$ and 2.5 msec. Examining cuts 3 and 4 demonstrates that the plasma is diverted upward in such a way as to balance the x momentum of the beam-plasma system. In examining Figs. 5(a) and 5(b) in detail we notice the following characteristics. First, the lateral plasma velocity along

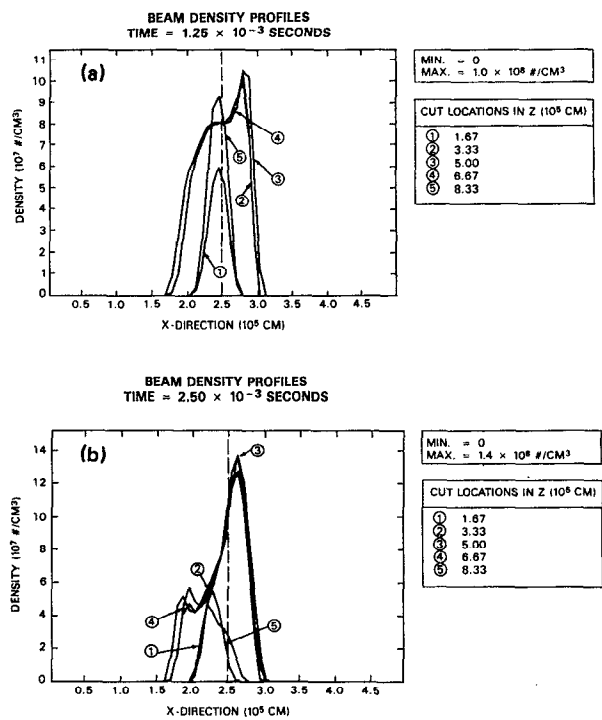


FIG. 4. Vertical beam density profiles at the diagnostic locations for run #1. (a) At $t = 1.25$ msec. (b) At $t = 2.5$ msec.

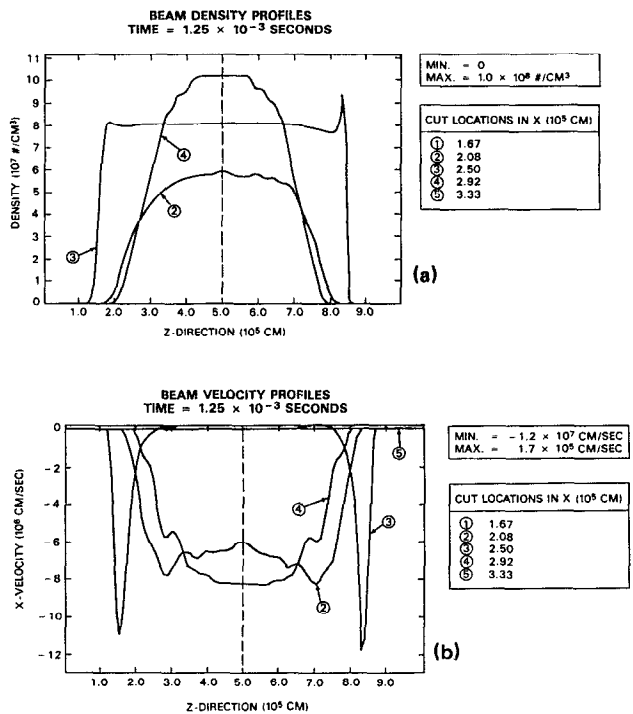


FIG. 5. Horizontal profile of the ambient plasma lateral velocity for run #1. (a) At $t = 1.224$ msec. (b) At $t = 2.5$ msec.

cut 1 that lies below the beam is basically unaffected; the plasma follows its original flow in this region. Second, there is strong upward diversion in the plasma flow along cuts 2, 3, and 4, which pass through the beam. The plasma diversion occurs throughout the region occupied by the beam, and is not confined to the front of the interaction. As a result plasma and field that were initially located inside the beam region are moved upward, resulting in progressively lower magnetic field and plasma density values inside the beam

region. As we will see the conclusion that the plasma density and the magnetic field inside the beam are decreasing with time has rather profound implications.

We proceed next to examine the structure of the electromagnetic fields that cause the plasma diversion and the associated beam erosion. The initially uniform magnetic field has been modified, as shown in the isomagnetic $\Delta B(x,z) = B(x,z) - B_0$ contours of Fig. 6. Notice that at the beam front there is a field compression with maximum

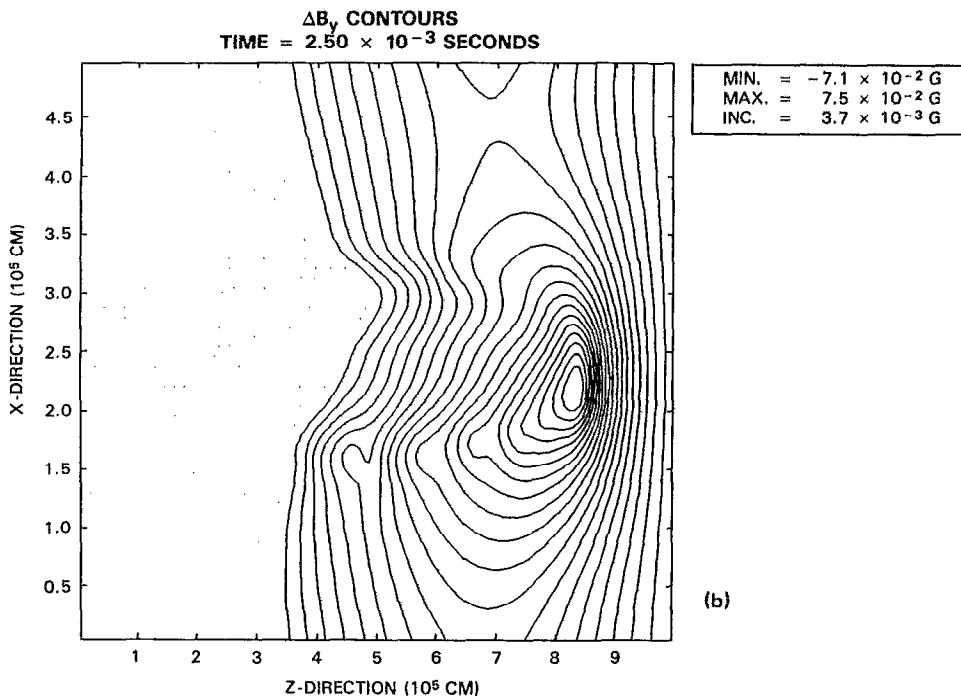
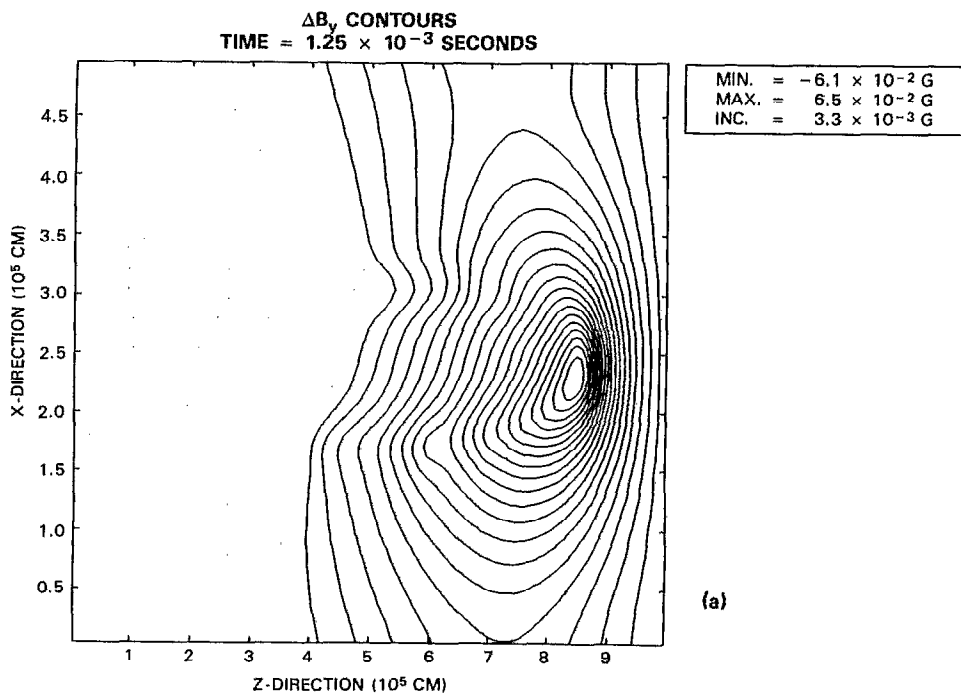


FIG. 6. Isomagnetic contours ΔB for run #1. (Solid lines represent compression of the magnetic field.) (a) At $t = 1.25$ msec. (b) At $t = 2.5$ msec.

compression of the order $\Delta B/B_0 = 2.3 \times 10^{-1}$ followed by a comparable diamagnetic reduction at the back of the beam. From Figs. 6(a) and 6(b) we notice that the magnetic configuration has achieved an essentially stationary state, which was established as early as $\Omega_b t \lesssim 0.3$. Furthermore, since the electrons and the magnetic field move together, the field compression is accompanied by a reduction in the flow velocity of the electrons. A net $\mathbf{u} \times \Delta \mathbf{B}$ force is thus produced, which results in the observed upward plasma diversion. In the laboratory frame this is equivalent to the beam front diverting the plasma ions sideways while the main beam follows an essentially ballistic trajectory. The beam front suffers an erosion since momentum is required to balance the flow diversion. For $\beta_b \gg 1$ the rate of erosion is rather small and long range beam propagation can be achieved. It is essential to notice the highly asymmetric character of the established steady state, which is contrary to the one expected from fluid or MHD models. We will return to this point later on.

To understand the phenomenology controlling the scaling of the ballistic propagation time scale, we examine the horizontal beam density profiles [Figs. 7(a) and 8(a)] and lateral velocity profiles [Figs. 7(b) and 8(b)] at the center cut (location #3, representing the maximum of the beam density and momentum flux) at times 1.25 and 2.5 msec. A comparison of Figs. 6(a), 7(a), and 8(a), in conjunction with Figs. 4(a) and 4(b) shows that the beam density has been compressed at the center point, while the longitudinal length is preserved. Furthermore, Figs. 7(b) and 8(b) dem-

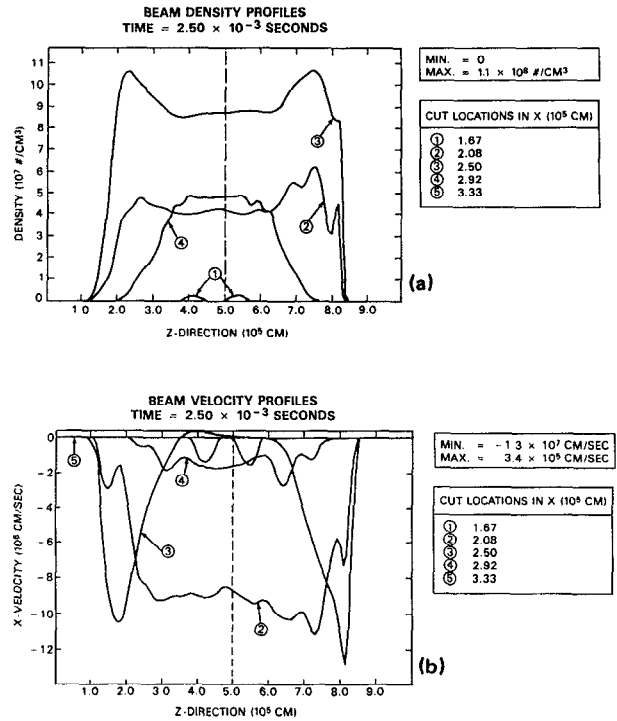


FIG. 8. Same as Fig. 7 at $t = 2.5$ msec.

onstrate that the center of the beam (cut 3) follows a ballistic trajectory (i.e., $u_x = 0$), except at the front and the rear. The front of the beam is eroding at a downward velocity that has saturated at a value $u_x \approx 10^7$ cm/sec. As can be seen by examining the horizontal downward velocity profile at location #3 in Figs. 7(b) and 8(b) the erosion is penetrating backward toward the beam center.

Let us summarize the key results of run #1 described previously in terms of a simplified model. In the beam frame the ambient magnetized plasma flows with a cross-field velocity $\mathbf{u}_p = -u_b \hat{e}_z$, with the aid of a motional electric field $\mathbf{E} = -(\mathbf{u}_e \times \mathbf{B}_0)/c = -\hat{e}_x (u_b B_0)/c$, where \mathbf{u}_e is the fluid velocity of the plasma electrons and of the magnetic flux (i.e., \mathbf{u}_e is the plasma frame velocity). The equations of motion of the background plasma ions (charge e , mass M_p) are

$$\frac{du_x}{dt} = \frac{e}{M_p} \left(E_x - \frac{u_x B_y}{c} \right), \quad (4a)$$

$$\frac{du_z}{dt} = \frac{e}{M_p} \left(E_z + \frac{u_x B_y}{c} \right). \quad (4b)$$

The value of the motional electric field $E_x(z)$ is given by

$$\hat{e}_x(z) = -\frac{\mathbf{u}_e(z) m \hat{e}_y B(z)}{c} = \hat{e}_x \frac{u_e(z) B(z)}{c}. \quad (5)$$

In the region $z > 0$ ahead of the beam-plasma interface, $u_e(z) = -u_b$ and $u_z = -u_b$ so that the rhs of (4a) is zero. Namely, the ions, the electrons, and the flux follow straight

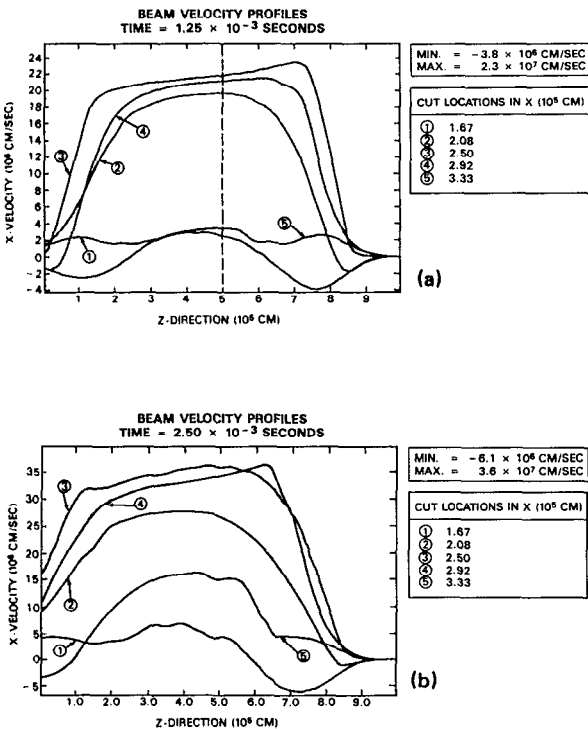


FIG. 7. Horizontal profiles of the (a) beam density and (b) lateral velocity for run #1 at $t = 1.25$ msec.

ballistic orbits. At the plasma interface, $z \approx 0$, the fluid velocity u_e reduces to

$$u_e(z) = n_b u_b / [n_b + n_p(z)] \quad (6)$$

to maintain charge and current neutrality. This is accompanied by a diamagnetic current at the front and a field compression such that $B(z)/B_0 \approx 1 + n_b(z)/n_p$. From Eq. (4a) the reduction in $u_e(z)$ produces a net force $[e \Delta B(z)/M_0 c] u_b$ in the positive x direction that diverts the plasma ions upward. In a high β flow the electrons and the flux follow the ion path. For $\Delta \ll R_0$ a change of the plasma frame speed of the order $\Delta u_e / u_b \approx \Delta / R_0$ is sufficient to establish a quasistationary state in which the background is diverted in a highly asymmetric fashion around the beam. The stationary value of the $\Delta B / B_0$ compression is consistent with the $\Delta u_e / u_b \approx \Delta / R_0$ requirement. This, of course, implies that ΔB should be linearly dependent on u_b and Δ and weakly dependent on the other parameters. Other key elements of the model are (i) the interaction at the front prevents further interpenetration of the plasma and the beam; (ii) any plasma and field that initially penetrated the beam are flowing out of the beam region; and (iii) as long as a stationary field structure such as shown in Fig. 6 remains the beam will propagate ballistically. Front erosion leads to deterioration of the stationary structure and termination of the ballistic beam propagation mode.

The purpose of runs #2–#5 was to confirm some of the features described previously and determine the scaling laws that control the range of ballistic beam propagation. We examine separately the scaling with beam velocity and beam density.

Runs #1–#3 all have the same number of beam particles (4.8×10^{18}) or an equivalent $n_b/n_0 = 800$, but the flow velocity corresponds to 10^8 , 2×10^8 , and 4×10^8 cm/sec, respectively. Figures 9(a) and 9(b) show the horizontal profiles of the beam density and downward displacement at time $t = 1.25$ msec for run #2. The center density profile and center downward velocity are essentially similar to run #1. However, the erosion speed at the front of cut #3 [Fig. 9(b)] is almost a factor of 2 faster than in run #1 (i.e., 2×10^7 cm/sec vs 1.1×10^7 cm/sec). This is confirmed by referring to the same profiles at time $t = 2.5$ msec [Figs. 10(a) and 10(b)]. While there is still substantial beam density along the center cut #3 [Fig. 10(a)], the front has eroded to such an extent that the beam center is now drifting downward at a speed of 10^7 cm/sec. In the aforementioned two runs the erosion rate scales almost linearly with u_b . The same scaling is evident from an examination of run #3 ($u_b = 4 \times 10^8$ cm/sec). Figure 11 shows the density (a) and downward beam velocity (b) at an earlier time ($t = 0.75$ msec). While the density profile is similar to Figs. 7(a) and 10(a) at $t = 1.25$ msec, the downward erosion speed is now 4×10^7 cm/sec, again revealing linear scaling with beam velocity. As a result of the faster erosion rate the profiles at $t = 1.25$ msec (Fig. 12) are similar to the ones of run #2 at 2.5 msec (Fig. 11). By the time $t = 2.5$ msec the beam has been displaced and modified substantially. However, it has still maintained its plasmoid-like entity, although it is no longer following a ballistic propagation path [Fig. 13(a)].

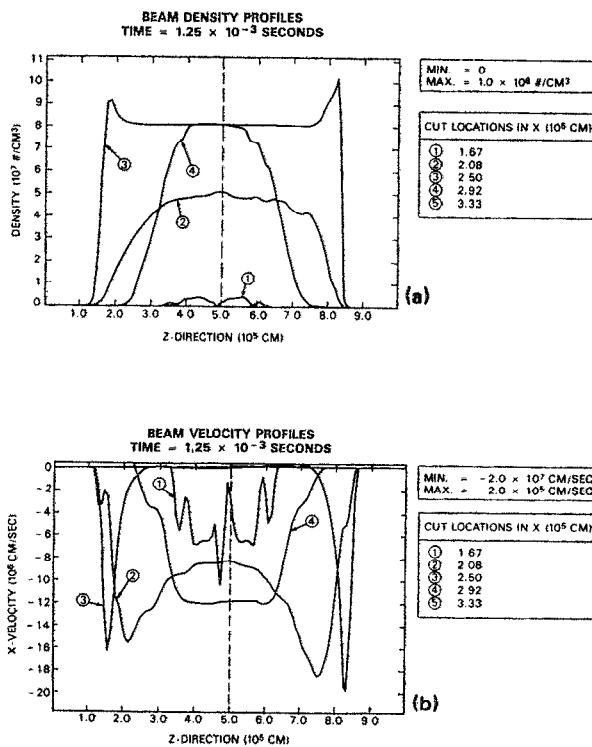


FIG. 9. Horizontal profiles of (a) the beam density and (b) lateral velocity for run #2 at $t = 1.25$ msec.

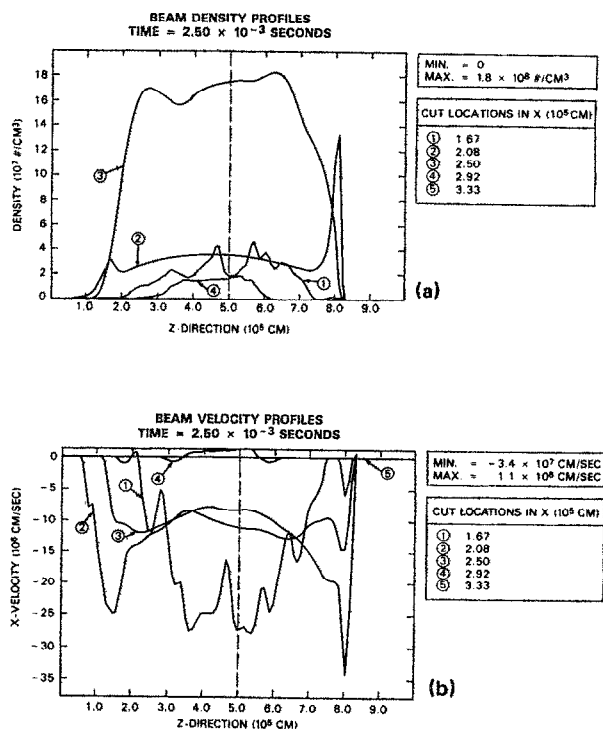


FIG. 10. Same as Fig. 9 at $t = 2.5$ msec.

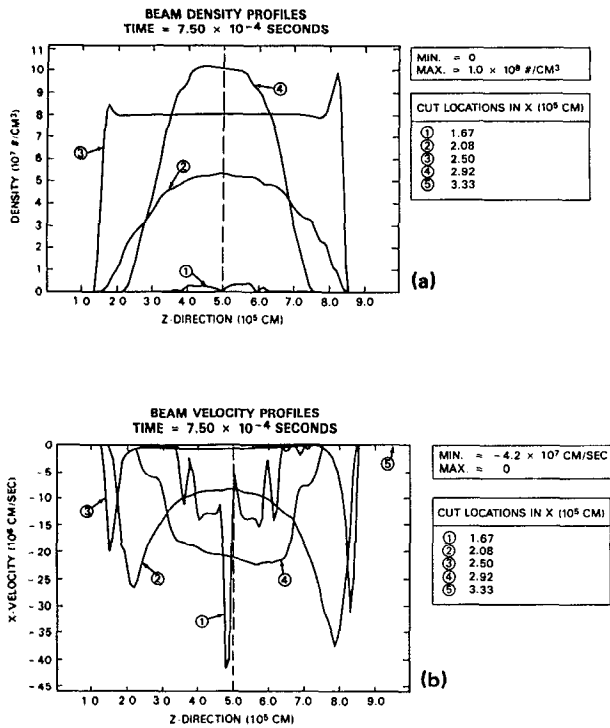


FIG. 11. Same as Fig. 10 for run #1 at $t = 0.75$ msec.

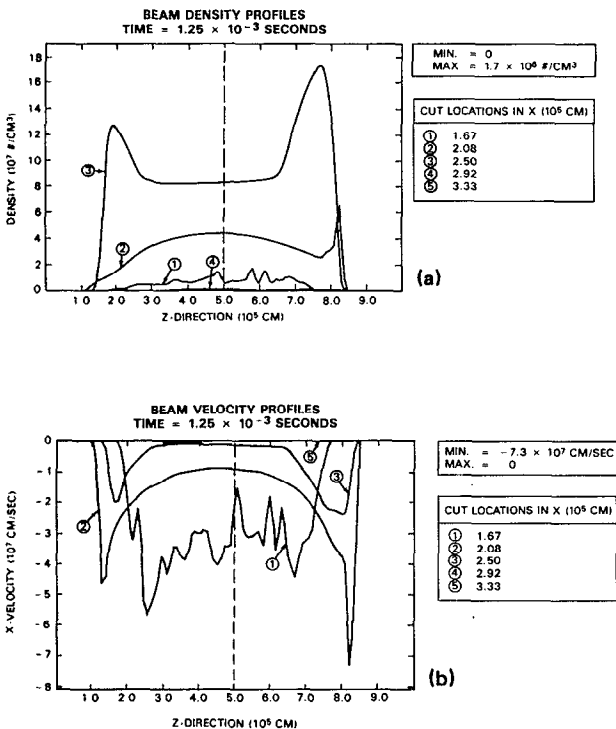


FIG. 12. Same as Fig. 11 at $t = 1.25$ msec.

Figure 13(b) shows ΔB contours at the same time. They should be compared with the contours of the ballistic propagation mode (Fig. 6). Finally, Figs. 14(a) and 14(b) show the plasma flow profiles at $t = 1.25$ msec for runs #2 and #3. It can be seen from these and Fig. 9(a) that, as expected from the previous results and momentum conservation, the diversion velocity of the plasma at the front as well as the outflow velocity of the plasma from the beam center scale almost linearly with u_b . It should be noted that for the previous runs the value of the magnetic field compression at the front also scales linearly with u_b .

Next we address scaling issues related to beam-to-plasma density ratios. Runs #1, #4, and #5 all have the same velocity $u_b = 10^8$ cm/sec, but the number of beam particles is 4.8×10^{18} #/cm³, 1.2×10^{18} , and 3×10^{17} , corresponding to $n_b/n_0 \approx 800, 200,$ and 50 . Figures 15(a), 15(b), 16(a) and 16(b) show horizontal profiles of beam density and lateral velocity for run #4 at $t = 1.25$ and 2.5 msec. A comparison of Fig. 15 with Fig. 7 shows that over the time scale of $t = 1.25$ msec ($\Omega_b t = 4$) the beam density profiles are basically self-similar for runs #1 and #4. However, in the lower density case (run #4), the center of the beam drifts with $u_x = 2 \times 10^6$ cm/sec while the front erosion speed is 1.7×10^7 cm/sec [Fig. 15(b)]. In comparing this with runs #1–#3 [Figs. 8(b), 9(b), and 11(b)] we note that for the high-density cases there was essentially no drift of the center of the beam before erosion. The front erosion speeds, however, were $10^7, 2 \times 10^7,$ and 4×10^7 cm/sec. Namely, a change in density by a factor of 4 resulted in a 70% change in the front erosion rate. Referring to Fig. 16 we note that while most of the energy density still remains at the beam center, a combination of a faster erosion rate and a larger downward displacement of the beam center will destroy the ballistic propagation mode. Figures 17(a) and 17(b) show the velocity displacement profiles of the ambient plasma at $t = 1.25$ and 2.5 msec for run #4. Notice that they are qualitatively and quantitatively similar to the ones for run #1 [Figs. 5(a) and 5(b)]. Furthermore, the outflow shows constant acceleration. The previous scalings with density continue for the case of run #5 [Figs. 18(a), 18(b), 19(a), 19(b)], which has a factor of 4 fewer beam particles than run #4 and 16 times fewer than run #1. It should finally be noted that for the previous runs the value of the maximum field compression was approximately the same.

In summary, the simulations previously described demonstrate that the presence of a propagating ion beam with $n_b \gg n_0$ sets up an electrodynamic configuration that laterally diverts the ambient plasma in such a fashion that no plasma penetration through the main beam occurs. The lateral diversion speed scales linearly with the beam velocity and is independent of the beam-to-plasma density ratio. Although specific simulation studies with various values of the ambient magnetic field B_0 were not performed, the physical understanding dictates linear scaling of the lateral speed with B_0 . The beam responds to this configuration in a manner that is consistent with conservation of momentum in the plasma frame. As a consequence of this for time scales that are shorter than the front erosion time (i.e., for long thin beams) and for $n_b M_b \gg n_0 M_0$, the plasma is evacuated from

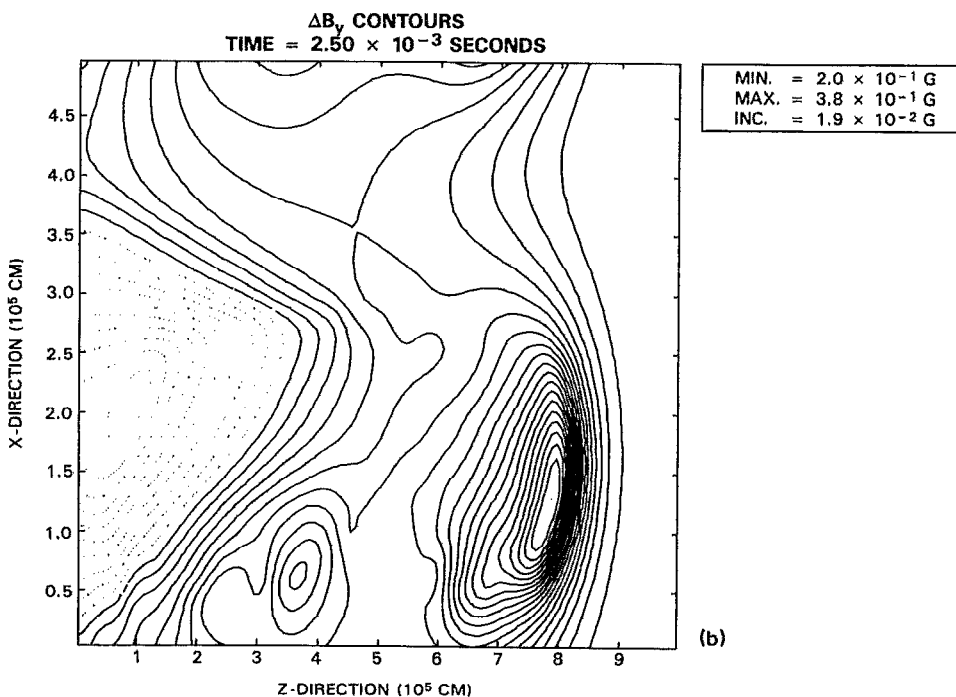
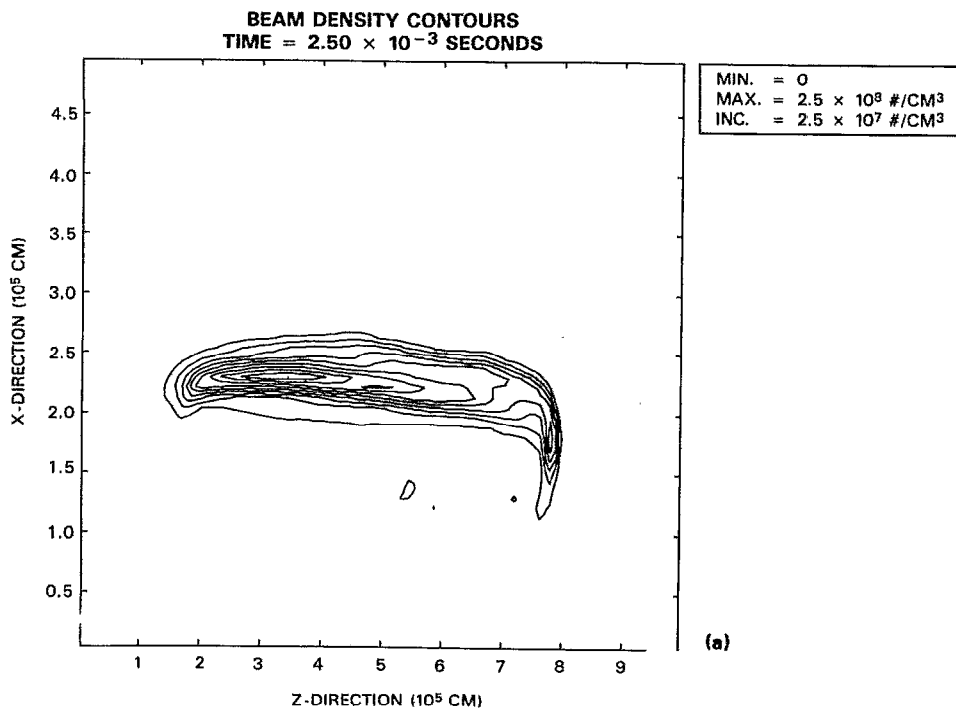


FIG. 13. (a) Isodensity and (b) isomagnetic ΔB contours for run #3 at $t = 2.5$ msec (solid lines represent compression while dashed lines represent depression of the ambient magnetic field).

the central beam region with minimum beam displacement. In fact, the simulations show that the dynamics of the system are such that focusing is produced at the center while momentum is balanced by shedding of surface particles from

the beam. The beam will subsequently follow a ballistic path until erosion of the front destroys it. The erosion rate was found to scale linearly with the beam velocity and by the previous argument with B_0 .

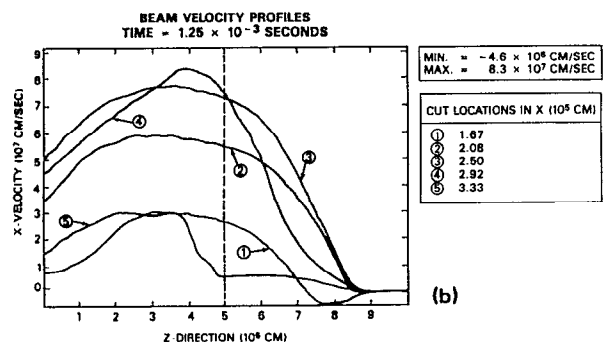
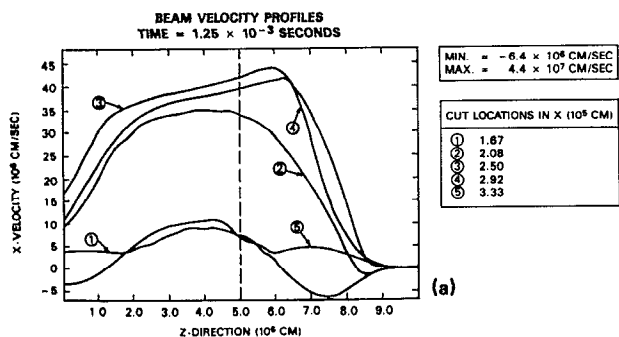


FIG. 14. Horizontal profile of the ambient plasma lateral velocity at $t = 1.25$ msec. (a) For run #2. (b) For run #3.

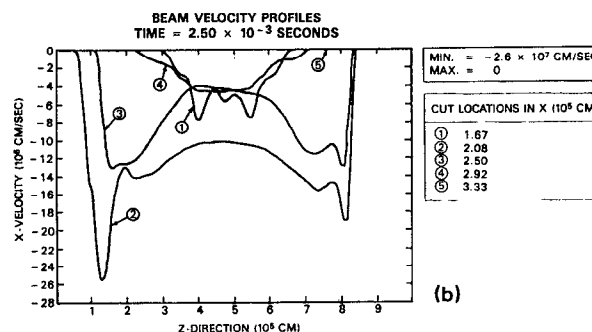
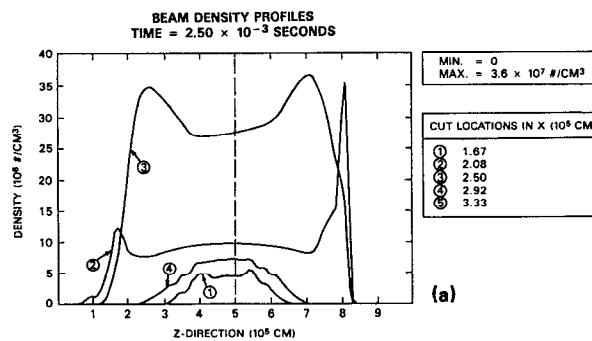


FIG. 16. Horizontal profiles of (a) the beam density and (b) lateral velocity for run #4 at $t = 2.5$ msec.

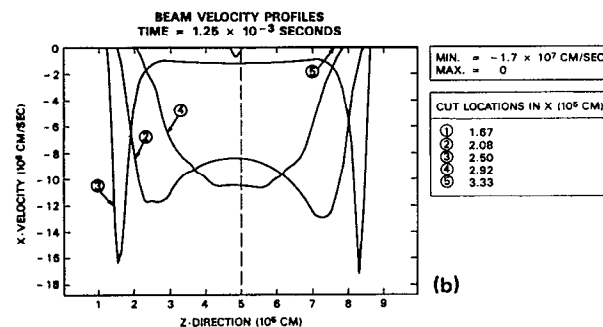
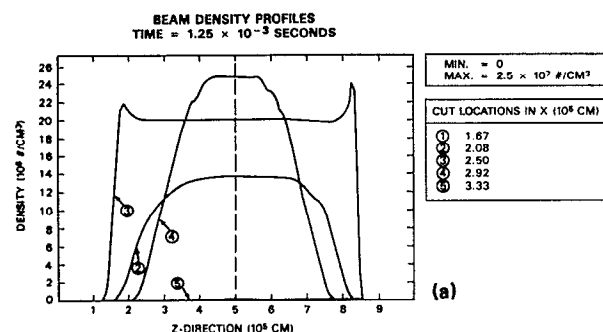


FIG. 15. Horizontal profiles of (a) the beam density and (b) lateral velocity for run #4 at $t = 1.25$ msec.

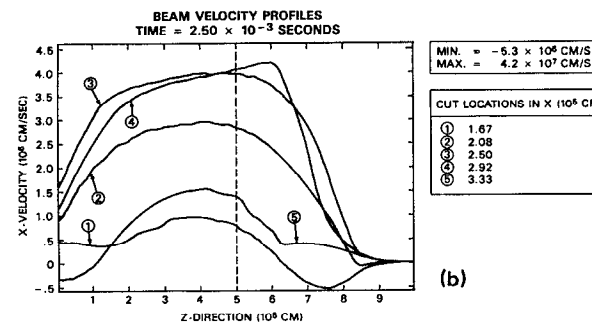
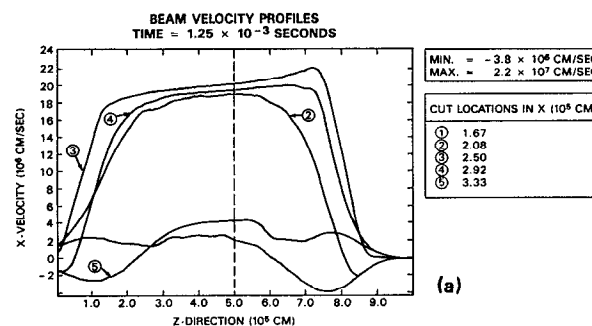


FIG. 17. Horizontal profiles of the ambient plasma lateral velocity for run #4. (a) $t = 1.25$ msec; (b) $t = 2.5$ msec.

IV. AN ANALYTIC VLASOV-FLUID MODEL OF THE INTERACTION

In Sec. III we presented the results of a comprehensive set of hybrid computer simulations for the case of an initially uniform magnetoplasma flowing past a neutralized ion beam at super-Alfvénic speeds. As mentioned in Secs. I and II, our purpose is to produce a study of the beam propagation under a wide parameter range and beam injection conditions. Time step constraints, such as discussed in Sec. II, prevent us at the present time from carrying out a wider range of investigations. We, however, feel that the investigations presented in Sec. III, supplemented by a comprehensive analytic understanding, will allow us to obtain the desired results. It is, thus, the purpose of this section to provide a theoretical framework for describing the limiting cases of the steady state cross-field ion beam propagation. In describing the model we shall use the subscript “ j ” to denote the various plasma and beam constituents. The basic model treats the beam ions ($j = b$) with the Vlasov equation; the background plasma flowing to the left with $\mathbf{u}_p = \mathbf{u}_e = -\mathbf{u}_b = -u_b \hat{e}_z$ as $z \rightarrow \infty$ (Fig. 20). The electrons ($j = e$) are treated as a cold macroscopic fluid immersed in a magnetic field. Local charge neutrality with

$$n_e(x) = n_b(x) + n_p(x) \quad (7)$$

is assumed everywhere. This restricts our analysis to scale lengths much greater than the Debye length. The analysis is again carried out in the beam frame with the background plasma flowing to the left with $\mathbf{u}_p = \mathbf{u}_e = -\mathbf{u}_b = -u_b \hat{e}_z$ as $z \rightarrow \infty$ (Fig. 20). The electrons ($j = e$) are treated as a cold, massless fluid moving with velocity

$$\mathbf{u}_e = \mathbf{u}_E \equiv (c/B_y) \mathbf{E} \times \hat{e}_y, \quad (8)$$

and satisfying the continuity equation

$$\mathbf{u}_E \cdot \nabla (n_e/B_y) = 0, \quad (9)$$

where $n_e(x, z)$ is the electron density and $\mathbf{E} = -\nabla\phi(x, z)$ is the electric field.

The beam ions ($j = b$) are described by the perpendicular distribution function $F_b(H_\perp/T_b)$, where $H_\perp = M_b v_\perp^2/2 + e\phi(x, z)$. The corresponding density profile $n_b(x, z)$ and perpendicular pressure profile $P_b(x, z)$ are given self-consistently by

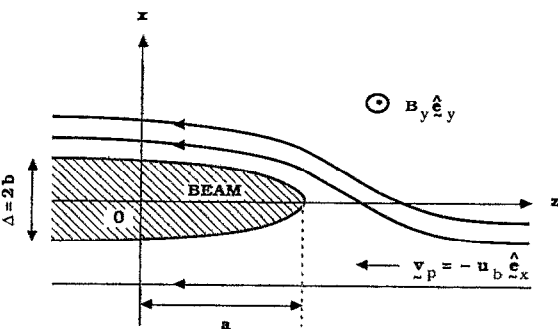


FIG. 20. The beam configuration used in analytic studies.

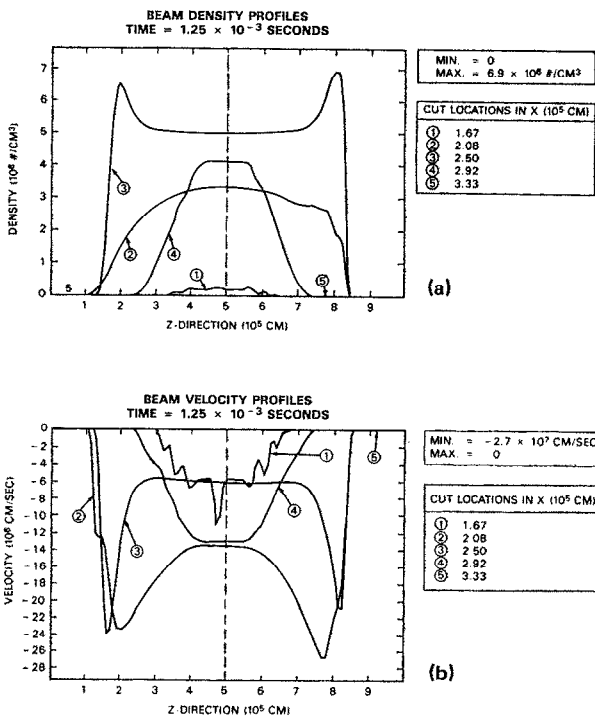


FIG. 18. Horizontal profiles of (a) the beam density and (b) lateral velocity for run #5 at $t = 1.25$ msec.

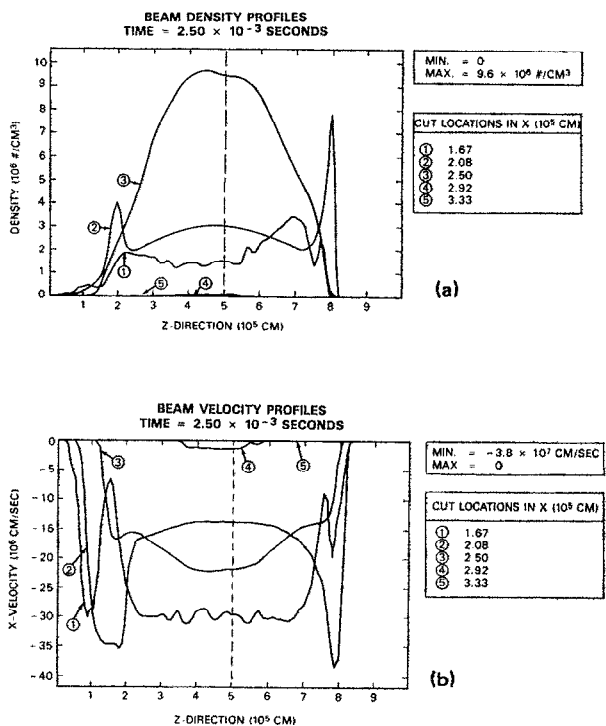


FIG. 19. Horizontal profiles of (a) the beam density and (b) lateral velocity for run #5 at $t = 2.5$ msec.

$$n_b = \hat{n}_b \int_0^\infty du F_b \left(u + \frac{e\phi}{T_b} \right), \quad (10)$$

$$P_b = \hat{n}_b T_b \int_0^\infty du u F_b \left(u + \frac{e\phi}{T_b} \right), \quad (11)$$

which also satisfy the force balance equation

$$\nabla P_b = n_b |e| \mathbf{E}, \quad (12)$$

where $\mathbf{E} = -\nabla\phi$.

The background plasma ions ($j=p$) are treated as a cold fluid with cross-field flow velocity \mathbf{u}_p satisfying

$$n_p M_p \mathbf{u}_p \cdot \nabla \mathbf{u}_p = n_p e [\mathbf{E} + (\mathbf{u}_p \times B_y \hat{e}_y)/c], \quad (13)$$

and the continuity equation

$$\nabla \cdot (n_p \mathbf{u}_p) = 0. \quad (14)$$

The electric field is described by $\nabla \times \mathbf{E} = 0$ and $\mathbf{E} = -\nabla\phi$. Local charge neutrality is assumed, $n_e = n_p + n_b$, and $B_y(x,z)$ is related self-consistently to the ion beam pressure and the background ion flow by

$$\nabla (B_y^2/8\pi + P_b) = -n_p m_p \mathbf{u}_p \cdot \nabla \mathbf{u}_p. \quad (15)$$

We next examine a simple limiting case using Eqs. (7)–(15). We first consider the case where there is no ambient plasma, i.e., $n_p = 0$. Some key physics issues can be illustrated by referring to a distribution of the beam ions given by

$$F_b \left(\frac{H_1}{T_b} \right) = \exp \left(-\frac{M_b v_1^2}{2T_b} - \frac{e\phi}{T_b} \right), \quad (16)$$

and an elliptical beam density profile given by

$$n_e(x,z) = \hat{n}_e \exp(-z^2/a^2 - x^2/b^2). \quad (17)$$

Notice that $n_e(x,z) = \text{const}$ on surfaces with $x^2/b^2 + z^2/a^2 = \text{const}$. Substituting (16) into (10) and (11) we find

$$n_b(x,z) = \hat{n}_b \exp(-e\phi/T_b) \quad (18)$$

and $P_b(x,z) = n_b(x,z) T_b$, which corresponds to an isothermal equilibrium with temperature T_b . From Eqs. (17) and (18) and the local neutrality condition Eq. (7) we find the distribution of the potential to be

$$\phi(x,z) = \frac{T_b}{|e|} \left(\frac{z^2}{a^2} + \frac{x^2}{b^2} \right), \quad (19)$$

and the corresponding self-consistent electric field

$$\mathbf{E} = -\frac{2T_b}{|e|} \left(\frac{z}{a^2} \hat{e}_z + \frac{x}{b^2} \hat{e}_x \right). \quad (20)$$

The magnetic field $B_y(x,z)$ can be calculated from the pressure balance Eq. (15) with $n_p = 0$ and $P_b(x,z) = n_b(x,z) T_b$ as

$$B_y(x,z) = B_0 \left[1 - \frac{8\pi \hat{n}_b T_b}{B_0^2} \exp \left(-\frac{z^2}{a^2} - \frac{x^2}{b^2} \right) \right]^{1/2}. \quad (21)$$

The magnetic field depression is produced as follows. From Maxwell's equation,

$$\nabla \times B_y \hat{e}_y = - (4\pi/c) n_e |e| c \mathbf{E} \times \hat{e}_y / B_y,$$

giving $(B_y/4\pi) \nabla B_y = -n_e |e| l \mathbf{E}$. Equation (21) follows because $n_e = n_b$ and $n_b e \mathbf{E} = \nabla P_b = (-B_y/4\pi) \nabla B_y$. The essential physics aspect of the example is that the extent of diamagnetism depends on the ion energy transverse to the magnetic field as measured from the reference frame where the magnetic field is stationary, i.e., the plasma frame. This appears as an ion finite beta effect, $\beta_i \approx 8\pi \hat{n}_b T_b / B_0^2$ in Eq. (21). The physics can be equivalently described by considering each ion as having a magnetic moment proportional to v_1^2/B_0 and summing the diamagnetic currents over the distribution functions, as described in Spitzer.²⁸ Although the present analysis considered cold electrons, which therefore produce a negligible diamagnetic current, it can be extended in an obvious fashion by considering an electron distribution similar to (16). In this case the magnetic field will again be given by Eq. (21) with T_b replaced by $T_b + T_e$, where T_e is the electron temperature. The following conclusions result directly from the above analysis.

An ion beam injected into a vacuum magnetic field will shield and exclude the field if

$$\beta_e + \beta_i = 8\pi n_b (T_e + T_b) / B^2 > 1.$$

However, the time scale over which the effect takes place is radically different, depending on whether β_e or β_i dominates. For the electron case the time scale is of the order of few times $1/\Omega_e$, while in the ion case it scales with the ion gyrotime $1/\Omega_b$. Furthermore, for situations where $a < R_b$ only the electron diamagnetism is important and the magnetic field will not be shielded unless $\beta_e > 1$.

Let us next examine the level of diamagnetism for the case of injection into a magnetized plasma with $n_p < n_b$. If $\beta_e > 1$ the situation is similar to the vacuum case. For $\beta_e < 1$, we must again rely on the ion beam driving the appropriate diamagnetic currents. The basic difference between the vacuum and the ambient plasma case is the velocity of the plasma frame. The velocity of the plasma frame is

$$\mathbf{u}_{ez} = [n_b / (n_p + n_b)] \mathbf{u}_b. \quad (22)$$

In assessing the role of ions in the formation of diamagnetic current for cold ions and electrons the relevant energy that will be compared to $B_0^2/8\pi$ is the ion energy with respect to the plasma frame, given by

$$\epsilon_i = \frac{1}{2} n_b M_b (u_b - u_{ez})^2 + \frac{1}{2} n_p M_p u_{ez}^2, \quad (23a)$$

which for $n_b \gg n_p$ is

$$\epsilon_i = \frac{1}{2} n_b M_b u_b^2 (n_p/n_b)^2 + \frac{1}{2} n_p M_p u_b^2. \quad (23b)$$

For $\beta_b (n_p/n_b)^2 \gg 1$ the time scale over which the field will be shielded by the beam ions will depend on the beam ion gyrotime, while for $\frac{1}{2} n_b M_b u_b^2 \gg 1$ it will depend on the plasma ion gyrotime. Finally, for $\epsilon_i/B_0^2/8\pi < 1$, the magnetic field will not be shielded. The previous analysis defines the conditions following the beam injection. We proceed next to apply the Vlasov-fluid model given by Eqs. (7)–(15) to interpret the stationary state observed in the simulations discussed in Sec. III.

In general, one has to solve the Eqs. (7)–(15) subject to the following boundary conditions:

$$\mathbf{u}_p = \mathbf{u}_e \equiv \mathbf{u}_E = -\mathbf{u}_b \hat{e}_z \quad \text{for } z \rightarrow \pm \infty, \quad (24a)$$

$$n_p = n_e = n_0 \quad \text{for } z \rightarrow \pm \infty, \quad (24b)$$

and by specifying the ion beam distribution $F_b(H_i/T_b)$. For the present purposes, we use the model to interpret quantitatively certain fundamental properties of flow observed in the simulations of Sec. III.

In Cartesian coordinates the two components of the equilibrium force balance equation (13) can be expressed as

$$\left(u_{px} \frac{\partial}{\partial x} + u_{pz} \frac{\partial}{\partial z}\right) u_{px} = \frac{e}{M_p} \left(E_x - \frac{u_{px} B_y}{c}\right), \quad (25)$$

$$\left(u_{px} \frac{\partial}{\partial x} + u_{pz} \frac{\partial}{\partial z}\right) u_{pz} = \frac{e}{M_p} \left(E_z + \frac{u_{px} B_y}{c}\right), \quad (26)$$

in the region where the ion density $n_p(x,z)$ is nonzero. On the other hand, from $\mathbf{E} + \mathbf{u}_e \times \mathbf{B}_y \hat{e}_y / c = 0$, the electron flow is described by

$$u_{ex} = u_{E_x} \equiv cE_z / B_y, \quad (27)$$

$$u_{ez} = u_{E_z} \equiv cE_x / B_y. \quad (28)$$

Moreover, the continuity equations for the electrons and the background plasma ions are given by

$$\frac{\partial}{\partial x} (n_e u_{Ex}) + \frac{\partial}{\partial z} (n_e u_{Ez}) = 0, \quad (29)$$

$$\frac{\partial}{\partial x} (n_p u_{px}) + \frac{\partial}{\partial z} (n_p u_{pz}) = 0. \quad (30)$$

The magnetic field profile $B_y(x,z)$ is generally related to other plasma properties by $\nabla(B_y^2/8\pi + P_b) = n_p m_p \mathbf{u}_p \cdot \nabla \mathbf{u}_p$ [Eq. (15)]. For the present purposes, however, we use the more rudimentary form of Maxwell's equation given by $\nabla B_y \times \hat{e}_y = (4\pi e/c)(n_p \mathbf{u}_p - n_e \mathbf{u}_E)$. Enforcing local charge neutrality, $n_c(x,z) = n_p(x,z) + n_b(x,z)$, we obtain

$$\frac{\partial B_y}{\partial z} = \frac{4\pi e}{c} \left[-n_p(u_{px} - u_{Ex}) + n_b u_{Ex} \right], \quad (31)$$

$$\frac{\partial B_y}{\partial x} = \frac{4\pi e}{c} \left[-n_p(u_{pz} - u_{Ez}) + n_b u_{Ez} \right]. \quad (32)$$

Finally, for specified ion beam distribution function $F_b(H_i/T_b)$, the corresponding density profile $n_b(x,z)$ and pressure profile $P_b(x,z)$ are determined self-consistently from Eqs. (10) and (11), which are also consistent with $\nabla P_b = n_b e \mathbf{E}$.

To determine detailed properties of the background plasma flow past the plasmoid, Eqs. (25)–(32) and Eqs. (10) and (11) should generally be solved numerically subject to the boundary conditions in Eqs. (24). We use this model, however, only to make simple analytical estimates of the deflection of the background plasma by the plasmoid. In this regard, it is convenient to eliminate E_x and E_z in Eqs. (25) and (26) by means of Eqs. (27) and (28). This readily gives the components of acceleration as

$$a_{pz} \equiv \left(u_{px} \frac{\partial}{\partial x} + u_{pz} \frac{\partial}{\partial z}\right) u_{pz} = \frac{eB_y}{M_p c} (u_{px} - u_{Ex}), \quad (33)$$

$$a_{px} \equiv \left(u_{px} \frac{\partial}{\partial x} + u_{pz} \frac{\partial}{\partial z}\right) u_{px} = \frac{eB_y}{M_p c} (u_{pz} - u_{Ez}), \quad (34)$$

which are equivalent to Eqs. (25) and (26). We are interested in situations where $\beta_b \gg 1$ and $\Delta = 2b < R_0$. Because the directed velocity in the negative z direction is large and the dimension of the plasmoid in the x direction is narrow, only a small change in plasma flow velocity in the x direction is required to divert the flow around the plasmoid. Denoting $u_{px} = \Delta u_{px}$ and $u_{Ex} = \Delta u_{Ex}$, this corresponds to

$$|\Delta u_{px}|, \quad |\Delta u_{Ex}| < u_b. \quad (35)$$

To estimate the deflection of the background plasma, we now focus attention on the region

$$z > a, \\ -b < x < b, \quad (36)$$

where the background plasma is streaming toward the beam from the right (Fig. 20). Although the beam ion density is large ($n_b \gg n_p$) in the core region ($z^2 < a^2$ and $x^2 < b^2$), it is assumed that the density profile $n_b(x,z)$ is diffuse and extends at reduced levels ($n_b < n_p$) well into the region described by Eq. (36). We now examine Eqs. (29)–(34) sufficiently far to the right of the beam that the deflection of the flow in the x direction has just begun, and $|\Delta u_{px}|$ and $|\Delta u_{Ex}|$ are small in comparison with u_b . To leading order, we therefore neglect the terms $(\partial/\partial x)(n_e \Delta u_{Ex})$ and $(\partial/\partial x)(n_p \Delta u_{px})$ in the continuity equations (29) and (30), which gives

$$(n_b + n_p) u_{Ez} = n_0 u_b, \\ n_p u_{pz} = n_0 u_b, \quad (37)$$

in the region sufficiently far to the right of the beam. Here, n_0 and $-u_b$ are the (constant) values of the background plasma density and flow velocity as $z \rightarrow \infty$. Moreover, use has been made in Eq. (37) of equilibrium charge neutrality, $n_c(x,z) = n_b(x,z) + n_p(x,z)$. Equation (37) readily gives the approximate result

$$n_p (u_{pz} - u_{Ez}) = n_b u_{Ez} \quad (38)$$

in the region sufficiently far to the right of the plasmoid.

We estimate $u_{Ez} = -u_b$ on the right-hand side of Eq. (34), which gives

$$u_{pz} - u_{Ez} = -(n_b/n_p) u_b. \quad (39)$$

Because as follows from Eq. (39) $(u_{pz} - u_{Ez}) < 0$, we conclude that the plasma ions are flowing somewhat faster to the left (with average velocity u_{pz}) than the electrons (with average velocity u_{Ez}). Namely, the ions have a relative velocity with respect to the plasma frame. Moreover, as long as the observation region is sufficiently far out in the tail of density profile $n_b(x,z)$ of the beam ions that $n_b/n_p \ll 1$, we conclude from Eq. (39) that $|(u_{pz} - u_{Ez})/u_b| \ll 1$. Equations (34) and (39) can be used to estimate the characteristic size and polarity of the vertical acceleration $a_{px} = -u_b (\partial/\partial z) (\Delta u_{px})$ of a plasma ion fluid element in the region sufficiently far to the right of the beam. Substituting Eq. (39) into Eq. (34), we obtain the estimate

$$a_{px} = \frac{eB_y}{M_p c} \frac{n_b}{n_p} u_b. \quad (40)$$

Because the right-hand side of Eq. (40) is positive, we conclude that $a_{px} > 0$ and the plasma ions are deflected upward

as the background plasma flows toward the plasmoid in the region $z > a$ and $-b < x < b$. There is a concomitant slowing down of the background plasma ions in the z direction, which corresponds to $a_{pz} > 0$ as the plasma flow approaches the plasmoid. Consistent with $a_{pz} > 0$, we conclude from Eq. (17) that

$$\Delta u_{px} > \Delta u_{Ex}. \quad (41)$$

That is, as the ion fluid is deflected upward with $a_{px} > 0$ and $\Delta u_{px} > 0$, the electrons follow with somewhat slower flow velocity in the x direction.

The time τ_d to deflect the background plasma through a vertical distance $\Delta = 2b$ equal to the thickness of the beam ($\Delta \approx 2b$) can be readily estimated from $\Delta x = \bar{a}_{px} t^2 / z$. Here, \bar{a}_{px} denotes the average acceleration over the region of deflection. Treating a_{px} in Eq. (40) as approximately constant, we obtain

$$\Omega_0 \tau_d = [(4b\Omega_0 / u_b) (n_b / n_p)]^{1/2}. \quad (42)$$

It should also be noted from Eq. (31) that the x motion of the electrons and the background plasma ions produces a z variation of $B_y(x, z)$. Evidently, for $n_b \Delta u_{Ex} > 0$, the contribution from the final term on the right-hand side of Eq. (31) corresponds to $\partial B_y / \partial z > 0$. On the other hand, for $n_p (\Delta u_{px} - \Delta u_{Ex}) > 0$ [Eq. (41)], the contribution from the first term on the right-hand side of Eq. (32) corresponds to $\partial B_y / \partial z < 0$. Depending on the equilibrium profiles for n_b and n_p , the competition between these two terms can produce the profile shape for B_y in front of the beam illustrated in Fig. 21. These analytic results have been presented previously in an abbreviated form in Papadopoulos *et al.*²⁹

V. RANGE OF BALLISTIC ION BEAM PROPAGATION

From the simulations presented in Sec. III and the analysis of Sec. IV, we found that the motion of the beam is determined by two independent, at least to zero order, considerations.

(i) *By the interaction of the beam front with the ambient plasma.* As a result of this interaction the plasma is diverted away from the beam and interpenetration of the beam particles with plasma particles that were initially outside the beam is limited in a narrow region at the front. Furthermore, the magnetic flux is prevented from penetrating the beam. This occurs at the expense of beam front erosion, which is consistent with *local* conservation of momentum in the x

direction. The rate of erosion dz/dt can be estimated by simple energy and momentum considerations. From momentum conservation in the z direction we have

$$n_b M_b \frac{dz}{dt} = n_p M_p (u_b - u'_b), \quad (43)$$

where u'_b is the ambient plasma speed in the z direction after it has been diverted by the magnetic compression at the front. From conservation of energy,

$$u'_b{}^2 + u_x^2 = u_b^2, \quad (44)$$

where u_x is given from Eq. (25) as

$$u_x^2 = 2(e \Delta B / m_0 c) u_b \Delta \quad (45)$$

(i.e., the transverse energy equals the potential drop). For $u_x^2 \ll u_b^2$, i.e., $\Delta / R_0 \ll 1$, Eq. (44) becomes

$$u_x^2 = (u_b - u'_b) \approx 2u_b (u_b - u'_b),$$

so that

$$u_b - u'_b = \Omega_0 \frac{\Delta B}{B_0} \Delta. \quad (46)$$

The erosion rate is then found from Eqs. (43) and (46) to be

$$\frac{1}{u_b} \frac{dz}{dt} = \frac{n_p M_p}{n_b M_b} \frac{\Delta}{R_0} \frac{\Delta B}{B} < \frac{n_p M_p}{n_b M_b} \frac{\Delta}{R_0}. \quad (47)$$

Notice that for $\Delta / R_0 \ll 1$ and $n_p M_p \ll n_b M_b$ the erosion rate is a very small fraction of the beam speed. For a beam of length L we can define a beam erosion time as the time to penetrate to $z = L/2$ from the front. Then Eq. (48) gives an erosion time scale τ as

$$\Omega_b \tau > \frac{1}{2} \frac{n_b}{n_p} \frac{L}{\Delta}. \quad (48)$$

(ii) *By the motion of the main beam due to the presence of a laminar electric field E_x in the beam frame.* This lateral motion depends critically on whether plasma has penetrated the beam at $t = 0$. If there is no plasma inside the beam at $t = 0$, the field E_x will be totally shielded and the main beam will suffer no displacement. In this case the range of ballistic propagation is given by front erosion considerations only [Eqs. (47) and (48)]. In case that plasma with density n_p exists initially in the beam, the beam will suffer a displacement Δ of the order

$$\frac{\Delta x}{\Delta} \approx \frac{n_p M_p}{n_b M_b}, \quad (49)$$

as a result of the fact that the plasma and the field are evacuated from the beam region. The system will approach asymptotically a state of $n_p = 0$ inside the beam and complete field exclusion. The time scale for this is given by Eq. (42). By combining these two considerations we can predict the range of ballistic propagation under several conditions.

(a) If at $t = 0$ there is no plasma penetration in the beam the range will be controlled by the beam erosion rate [Eqs. (47) and (48)]. The ballistic propagation range will be

$$R \gtrsim \frac{1}{2} \frac{n_b}{n_p} \frac{L}{\Delta} R_b. \quad (50)$$

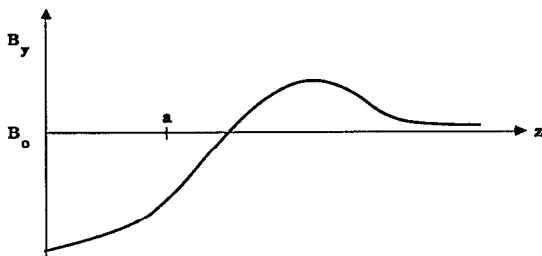


FIG. 21. The magnetic field configuration at the beam front.

For example, for a ratio $n_b/n_p \approx 100$ and $L/\Delta \approx 100$ the beam will propagate ballistically a distance of the order of 10^4 beam ion gyroradii. Furthermore, for a steady state injection situation Eq. (47) states that as long as the erosion rate is slower than the injection rate the beam will propagate ballistically at all times.

(b) If at $t = 0$ plasma has penetrated the beam it is critical to assess the importance of the beam motion from $t = 0$ until the ambient plasma has been evacuated. The asymptotic beam displacement will be given by Eq. (49). As long as $n_p M_p \ll n_b M_b$, $\Delta x \ll \Delta$ and the asymptotic beam displacement would not be significant. However, substantial deviation from the initial trajectory can occur since the beam has now a finite speed u_x , given by

$$u_x = - (n_p M_p / n_b M_b) u_{px}^\infty, \quad (51)$$

where u_{px}^∞ is the asymptotic value of the upward deviation of the plasma. Since $u_{px}^\infty \approx \Delta / R_0 u_b$, we find that

$$\frac{u_x}{u_b} \approx \frac{n_p M_p}{n_b M_b} \frac{\Delta}{R_0} \approx \frac{n_p}{n_b} \frac{\Delta}{U_b} \Omega_b. \quad (52)$$

Following this the beam will propagate ballistically controlled only by beam erosion considerations. The beam will deviate from its original path by an angle $\Delta\theta \approx n_p/n_b \Delta/R_b$. Notice that this *does not correspond* to beam divergence but to displacement of the beam center. The displacement Δs as a function of distance z will be given by $\Delta s = z\Delta\theta$, which corresponds to

$$\frac{\Delta s}{\Delta} = \frac{n_p}{n_b} \frac{z}{R_b}.$$

If the criterion of ballistic propagation is $\Delta s/\Delta < 1$, the range R will be given by

$$R \approx (n_b/n_p) R_b, \quad (53)$$

where n_p is the density of the plasma inside the beam at $t = 0$.

VI. CONCLUDING REMARKS

In this paper we examined the ballistic range of a neutralized ion beam with $\beta_b \gg 1$ propagating through a magnetoplasma. It was found that for $n_b/n_p \gg 1$ and $\Delta/R_0 \ll 1$, the beam will propagate by pushing the ambient medium to the side. No beam-plasma interpenetration will occur past the initial one. Furthermore, the plasma initially inside the beam will move out of the beam region on a time scale of a few ion gyrotimes. The initial beam divergence in the direction perpendicular to the magnetic field will thus be maintained. The range of ballistic beam propagation will be between a maximum value given by Eq. (50) for the case where the plasma was excluded from the beam region initially, to a minimum given by Eq. (53) in the opposite case. Ion beams in the mega-electron-volt range with current density of the order of 10^{-2} – 10^4 A/cm² will be able to propagate ballistically over distances of 500–2000 km. Several of the scaling laws developed here can be tested experimentally. In concluding we would mention that although the results presented here dealt with the case where the magnetic field was in the simulation plane, the existence of a magnetic field component in the x

direction does not alter the essential conclusions. The only difference will be that in the latter case the magnetic field lines diverted past the beam will show a small “draping.” This has been observed in initial results from three-dimensional simulations. Furthermore, since interpenetration is prevented we do not expect any significant effects resulting from microinstabilities. These issues will be discussed in a future publication.

ACKNOWLEDGMENTS

Discussions with Professor R. Sudan are gratefully acknowledged.

This work was supported by the U. S. Department of Energy under Contract No. DE-AC03-85SF15935.

- ¹S. Chapman and V. C. A. Ferraro, *Terr. Magn. Atmos. Electr.* **37**, 147 (1931).
- ²V. C. A. Ferraro, *J. Geophys. Res.* **57**, 15 (1952).
- ³J. L. Tuck, *Phys. Rev. Lett.* **3**, 313 (1959).
- ⁴S. Chapman, *Rev. Mod. Phys.* **32**, 919 (1960).
- ⁵P. Cargill, S. Sharma, and K. Papadopoulos, *Geophys. Res. Lett.* **15**, 740 (1988).
- ⁶W. H. Bostick, *Phys. Rev.* **104**, 292 (1956).
- ⁷G. Schmidt, *Phys. Fluids* **3**, 361 (1960).
- ⁸J. M. Dolique, *Compte Rendus* **256**, 3984 (1963).
- ⁹D. A. Baker and J. E. Hammel, *Phys. Fluids* **8**, 713 (1965).
- ¹⁰M. Baribaud, J. M. Dolique, and F. Zadworny, *Dynamics of Ionized Gases*, edited by M. J. Lighthill, I. Imsai, and H. Sato (Wiley, New York, 1971), p. 347.
- ¹¹W. A. Livesey and P. L. Pritchett, *Phys. Fluids B* **1**, 914 (1989).
- ¹²W. Peter and N. Rostoker, *Phys. Fluids* **25**, 730 (1982).
- ¹³M. Scholer, *Planet. Space Sci.* **18**, 977 (1970).
- ¹⁴R. Hong, F. J. Wessel, J. Song, A. Fisher, and N. Rostoker, *J. Appl. Phys.* **64**, 73 (1988).
- ¹⁵V. F. Birko and G. S. Kirchenko, *Sov. Phys. Tech. Phys.* **23**, 202 (1978).
- ¹⁶W. Shanahan (private communication).
- ¹⁷D. A. Gurnett, R. R. Anderson, B. Hausler, G. Haerendel, O. H. Bauer, R. A. Treumann, H. C. Koons, R. H. Holzworth, and H. Luhr, *Geophys. Res. Lett.* **12**, 851 (1986).
- ¹⁸G. Haerendel, G. Paschmann, W. Baumjohann, and C. W. Carlson, *Nature* **320**, 720 (1986).
- ¹⁹H. Luhr, D. J. Southwood, N. Kocker, M. W. Dunlop, W. A. C. Mier-Jedrzejowicz, R. P. Rijnbeek, M. Six, B. Hausler, and M. Acuna, *Nature* **320**, 708 (1986).
- ²⁰K. Papadopoulos and A. T. Y. Lui, *Geophys. Res. Lett.* **13**, 425 (1986).
- ²¹E. V. Mishin, R. A. Treumann, and V. Ya Kapitanov, *J. Geophys. Res.* **91**, 10183 (1986).
- ²²B. Ripin (private communication).
- ²³A. Mankofsky, R. N. Sudan, and J. Denavit, *J. Comput. Phys.* **70**, 89 (1987).
- ²⁴S. Humphries, *Appl. Phys. Lett.* **32**, 792 (1978).
- ²⁵S. Brandon (private communication).
- ²⁶M. M. Leroy, C. C. Goodrich, D. Winske, C. S. Wu, and K. Papadopoulos, *Geophys. Res. Lett.* **8**, 1269 (1981); *J. Geophys. Res.* **87**, 5081 (1982).
- ²⁷K. Papadopoulos, *Microinstabilities and Anomalous Transport in Collisionless Shocks in the Heliosphere: A Tutorial Review*, AGU Geophysical Monograph, edited by R. G. Stone and B. T. Tsurutani (AGU, Washington DC, 1985), Vol. 34, p. 59.
- ²⁸L. Spitzer, *Physics of Fully Ionized Gases* (Interscience, New York, 1962).
- ²⁹K. Papadopoulos, A. Mankofsky, and A. T. Drobot, *Phys. Rev. Lett.* **61**, 94 (1988); K. Papadopoulos, A. Mankofsky, and A. T. Drobot, *Plasma Waves and Instabilities at Comets and in Magnetospheres*, AGU Geophysical Monograph, edited by B. T. Tsurutani and H. Oya (AGU, Washington, DC, 1988), Vol. 53, p. 149.